INTEGR. COMP. BIOL., 42:981–987 (2002)

Riding the Waves: the Role of the Body Wave in Undulatory Fish Swimming[1]

ULRIKE K. MÜLLER,[2,*] EIZE J. STAMHUIS,[†] JOHN J. VIDELER[†]

*Department of Zoology, University of Cambridge, Downing Street, Cambridge CB2 3EJ, U.K.
†Department of Marine Biology, University of Groningen, P.O. Box 14, 9750 AA Haren, Gn, The Netherlands

SYNOPSIS. A continuously swimming mullet modulates its thrust production by changing slip-the ratio between its swimming speed *U* and the speed *V* with which the body wave travels down its body. This variation in thrust is reflected in the wake of the fish. We obtained 2-dimensional impressions of the wake behind a mullet swimming at a slip of 0.7 equivalent to active swimming, at a slip of 0.9 close to free-wheeling, and at a slip of 1.1 when the fish is braking. Independent of the slip, vortices are shed at the tail when the tail tip reaches its maximum lateral excursion. The manner in which the wake changes as it decays depends on the degree of slip: At a slip well below unity, the wake decays without any qualitative changes in shape, the medio-frontal cross section of the mature wake consists of a double row of alternating vortices separated by an undulating jet, and the angle between the jet flow and the mean path of motion is close to 45°; at a slip above unity, the vortices stretch out laterally and the mature wake resembles a single row of oval vortices with two vortex cores, and the jet between the vortices is almost perpendicular to the mean path of motion; the wake at slip of 0.9 exhibits a pattern intermediate between the wakes at slips 0.7 and 0.9 with slightly elongate vortices and a jet angle of 61°.

INTRODUCTION

Regular patterns are formed by vortices shed from fins and tails of swimming fish (Drucker and Lauder, 1999 and 2001; Hanke *et al.*, 2000; Müller *et al.*, 1997 and 1999; Nauen and Lauder, 2001; Wolfgang *et al.*, 1999; Wilga and Lauder, 2000). Medio-frontal cross-sections through the wake of undulatory swimmers often resemble a reverse Karman vortex street (Hanke *et al.*, 2000; Müller *et al.*, 1997; Wolfgang *et al.*, 1999). Mechanical model experiments (Ahlborn *et al.*, 1991; Anderson *et al.*, 1998; Cheng *et al.*, 1991; Hertel, 1966) and computational studies (*e.g.*, Streitlien and Triantafyllou, 1996) have established that wake shape and propulsion characteristics depend on the phase between pitch and heave of the oscillating propulsor and on the interaction between the wakes shed off the body, the fins and the tail.

In undulatory swimming, the body movements will generate a body wake, and the oscillating tail will generate its own tail wake. Experiments with a heaving and pitching plate (*e.g.*, Hertel, 1966, Anderson *et al.*, 1998) suggest fish are able to control propulsive performance of the tail by changing the phase between heave and pitch. For the body wave, changing slip *U*/*V*, the ratio of swimming speed *U* to the speed *V* of the body wave, is an equivalent mechanism; whether the body generates thrust- or drag-wakes depends on the slip. At slips below 1, the body wave travels down the body at a higher speed than the fish is swimming forward; the body wave moves backward relative to the water, accelerating the surrounding water backward and sideways, and the fish is generating thrust. At a slip of 1, the body wave travels backward at the same speed as the fish travels forward; the wave does not move relative to the water, accelerating the water only sideways, and the fish generates no shear relative to the water and no net thrust; it is only the fish's inertia that keeps the fish moving forward. At slips above 1, the fish swims faster than its body wave travels backwards; the body wave travels forward relative to the water, adding sideways and forward momentum to the water, and the fish gains backward momentum, and decelerates.

The flow generated by the different kinematic patterns has been examined on mechanical models simulating the tail beat of fish (Hertel, 1966; Ahlborn *et al.*, 1991; Triantafyllou *et al.*, 1993, Gopalkrishnan *et al.*, 1994, Anderson *et al.*, 1998). These experiments confirmed the hypotheses developed for fish swimming regarding the importance of the slip. At slips of less than 1 (Fig. 1), a waving plate sheds two rows of alternating vortices separated by an undulating, backward jet reflecting the backward momentum shed in the wake (Hertel, 1966). At a slip of 1, the wake consists of a single row of vortices and lateral jets, and no backward momentum is visible in the wake. At slips above 1, a von Kármán vortex street is shed with a double row of vortices associated with an undulating, forward jet; the wake has a forward momentum, and the waving plate is gaining backward momentum in return.

Undulatory swimmers display a range of slips (for a review see Videler, 1993). Mullet has a fusiform body shape with a pronounced tail fin, and generates a body wave with an amplitude increasing curvilinearly towards the tail (Müller *et al.*, 1997). In this study we use particle image velocimetry PIV to quantify the wake behind a mullet, and simultaneously record the swimming movements of the fish. This shows which types of wake are produced for different slips, and how these wakes are generated by the undulating body.

[1] From the Symposium *Dynamics and Energetics of Animal Swimming and Flying* presented at the Annual Meeting of the Society for Integrative and Comparative Biology, 2–6 January 2002, at Anaheim, California.

[2] E-mail: ukm20@cam.ac.uk

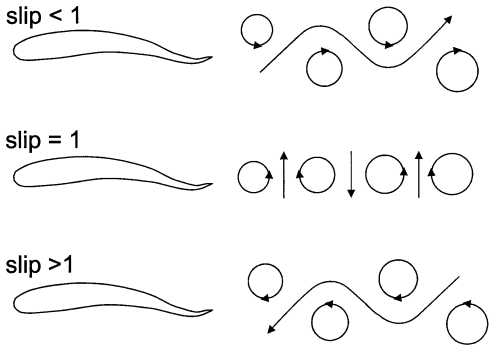

FIG. 1. Principle wake shapes, consisting of vortices (circles) and jets (waving lines), as observed by Hertel (1966) behind a flapping plate simulating the tail beat of a fish swimming at various slips. The arrows mark the flow direction. Wake of an actively flapping plate (slip < 1), a passively flapping plate (slip > 1) and a 'free-wheeling' flapping plate (slip $= 1$).

MATERIAL AND METHODS

The experiments were performed on thick-lipped mullet (*Chelon labrosus*). Two juvenile mullets (age 2 years, body length 0.12 m), bred in captivity, were kept in a 40 litre tank containing artificial sea water (salinity 30‰) at 22 ± 1°C.

The flow generated by the swimming fish was visualised using 2-dimensional particle image velocimetry PIV following Stamhuis and Videler (1995) and Müller *et al.* (1997). One fish was transferred to the filming tank (dimensions: 1.5 m × 0.5 m × 0.3 m) filled with water seeded with unexpanded polystyrene particles (VF 654, BASF, diameter 0.2 to 0.4 mm). The particles were illuminated in a horizontal plane by a 1 mm thick laser light sheet (krypton laser, $\lambda = 647$ nm, maximum power 0.8 W). The light sheet was in the middle of the water column, more than 5 tail-fin spans away from the surface and the bottom of the tank to avoid wall effects. Experiments lasted at most 2 hours. Only spontaneous swimming behaviour was recorded; we neither trained nor stimulated the fish in any way. A CCD camera (Adimec MX-12, with 50 mm lens) was mounted perpendicular to the light sheet to record top-view images of 512 × 512 pixels at a frequency of 25 images per second. The camera shutter was open for 8 m sec per frame to avoid motion blur of the particles. The flow fields obtained with our PIV setup are two-dimensional impressions in the medio-frontal plane of the fish. Morphological and kinematic parameters listed in Table 1 were obtained using image analysis software (TIM, Dutch Vision System) following Müller *et al.* (1997).

Hydrodynamic analysis

We conducted subimage cross-correlations on pairs of consecutive images to obtain a velocity vector field from the particle displacements (Chen *et al.*, 1993, Stamhuis and Videler 1995) using a subimage size of 39 by 39 pixels. The rotational flow component in the vortices was often too high for the cross-correlation to yield reliable results. These areas in the flow had to be analysed by tracking particle centroids manually (particle tracking velocimetry PTV). All vectors in one grid cell were averaged, and gaps in the resulting vector field were filled using a 2-dimensional spline interpolation technique (Stamhuis and Videler, 1995).

The wake was characterised by the following parameters: (a) the distance between vortex centres along and perpendicular to the mean path of motion; (b) the momentum angle φ between a vortex pair and the swimming direction; (c) the angle α between the direction of the jet and the mean path of motion. Consecutive counter-rotating vortices in the wake are assumed to form a vortex ring. We obtained the velocity profile of the vortices, the radius of the vortex ring R and the vortex core R_0.

We adapted the vortex ring model, developed for bird flight (Rayner 1979; Spedding *et al.*, 1984) to calculate the energy contained in the wake. We assumed the vortex rings to be circular and to contain all vorticity. The circulation Γ of the vortex was calculated as described in Müller *et al.* (1997). Undulatory swimming fish shed a chain of vortex rings (Blickhan *et al.*, 1992; Wolfgang *et al.*, 1999). The medio-frontal cross-sections obtained in this set-up contain the areas where two vortex rings overlap. The circulation Γ of two consecutive vortex rings can be assumed to be additive (Blickhan *et al.*, 1992). Hence, we modified the vortex ring model for birds, which was developed for single vortex rings, to suit a vortex chain as follows. We halved the circulation derived from the flow field when calculating vortex ring momentum I:

$$I = \rho_{water} \tfrac{1}{2} \Gamma \pi R^2, \quad (1)$$

TABLE 1. *Morphological and kinematic parameters.*

	Sequence 1	Sequence 2	Sequence 3
body length L (m)	0.126 ± 0.006 (7)	0.118 ± 0.003 (9)	0.111 ± 0.006 (6)
swimming speed U (m s^{-1})	0.173 ± 0.044 (9)	0.190 ± 0.020 (8)	0.307 ± 0.031 (5)
max. angle of tail with PoM* (deg)	31	32	39
tail beat frequency f (s^{-1})	3.86 ± 0.24 (4)	3.8 ± 1.14 (5)	3.82 ± 1.20 (3)
tail beat amplitude A (L)	0.09 ± 0.01 (5)	0.07 ± 0.01 (5)	0.08 ± 0.003 (3)
stride length λ_s (L)	0.53 ± 0.05 (17)	0.60 ± 0.07 (5)	0.70 ± 0.02 (3)
body wave length λ_b (L)	1.11 ± 0.19 (7)	1.09 ± 0.29 (5)	0.74 ± 0.24 (3)
slip U/V	0.7 ± 0.1 (8)	0.9 ± 0.1 (7)	1.1 ± 0.1 (4)
Strouhal number S	0.34	0.35	0.28

* PoM: path of motion.

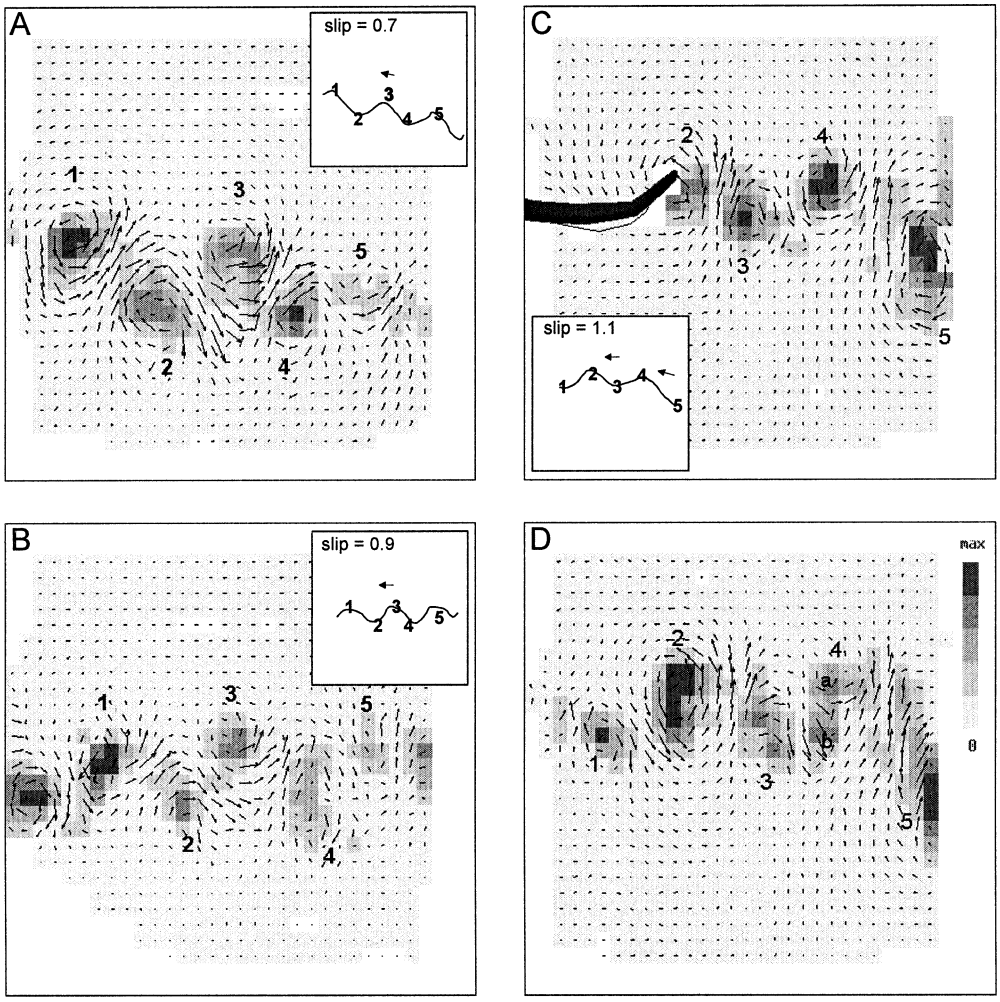

FIG. 2. Vorticity (grey values) in the vicinity of the fish (field of view 0.19 by 0.19 m); flow information obtained combining PIV and PTV. The arrows represent flow velocity in mm sec^{-1} (the length of the arrows is scaled up relative to the size of the field of view by a factor of 3). The vortices are numbered in reverse shedding order. The insets show the path of the tail tip in the field of view (line), the swimming direction (arrows) and the position of the vortex centres (numbers) 0.04 sec after being shed; the arrows indicate the swimming direction. (A) Wake behind an actively swimming fish (slip = 0.7). The most recently shed vortex "1" was shed 0.16 sec ago; vortex "5" 0.72 sec ago. (B) Wake behind a fish swimming at slip = 0.9. Vortices "1" and "5" were shed 0.12 s and 0.72 s ago, respectively. (C) Wake behind a decelerating fish (slip = 1.1). Vortex '2' is about to be shed at the tail. The fish initially turned through an angle of 23°. The analysed vortices were shed after the turn (the vortex to the very right was excluded from the analysis), when the fish swam at a slip of 1.1. (D) Wake from the same sequence as (C) 0.24 sec later; vortex "5" was shed 0.64 sec ago.

where ρ_{water} is the density of water. This leads to the thrust energy E_T:

$$E_T = 0.5 I\, U \sin\varphi. \tag{2}$$

With two vortices shed per tail beat cycle, this leads to thrust power P_T:

$$P_T = E_T 2f, \tag{3}$$

where f is the tail beat frequency.

RESULTS

Of 30 recorded sequences, three were selected in which the fish is swimming horizontally in the light sheet with the wake in full view of the camera. Of each sequence, up to 40 image pairs were analysed to quantify the swimming kinematics and the flow pattern generated by the fish. All mean values in the text are given with standard deviation.

Swimming kinematics

In all three sequences, the fish crosses the field of view from right to left, completing approximately 3 tail beat cycles. The kinematic profile of mullet is typical for carangiform swimmers (Table 1) (Wardle *et al.*, 1995; Müller *et al.*, 1997). The instantaneous swimming speed varies within a tail beat cycle by 25% of the mean swimming speed U. U does not change significantly between tail beat cycles ($P > 0.1$, $n = 3$). The slip in the sequences 1, 2 and 3 is 0.7 ± 0.1, 0.9 ± 0.1, and 1.1 ± 0.1, respectively.

The tail follows a sinusoidal path with tail beat am-

plitudes of 0.07 *L* (*U*/*V* = 0.9), 0.08 *L* (*U*/*V* = 1.1) and 0.09 *L* (*U*/*V* = 0.7) and stride lengths of 0.5 *L* (*U*/*V* = 0.7), 0.6 *L* (*U*/*V* = 0.9) and 0.7 *L* (*U*/*V* = 1.1) (Table 1 and Fig. 2, insets). The lateral velocity of the tail varies during the tail beat cycle between 0, when the tail reaches a lateral extreme, and more than 0.2 m sec^{-1}. The fish increases slip by reducing the speed with which the body wave travels down the body. This is turn decreases body wave length and increases the angle of attack of the tail.

Studies of fish flow fields (Müller *et al.*, 1997, 2001; present study) as well as model studies on heaving and pitching plates (Gopalkrishnan *et al.*, 1994; Streitlien and Triantafyllou, 1996; Anderson *et al.*, 1998) show at least three aspects of the body kinematics to be important for the flow patterns generated by the interaction between fish and water. First, the phase relationship between the heave and pitch of the tail. Second, the phase relationship between body wave and tail beat cycle. Third, the size of the lateral body wave amplitude relative to the width of the body, in particular the head.

(1) Heaving and pitching hydrofoil: a continuously swimming mullet has a reduced tail beat frequency of 1.6 to 2.4, and the tail reaches maximum heave when the pitch is 0° in the three analysed recordings. (2) The relationship between tail beat cycle and body wave: it is conceivable that the tail does not exactly follow the body wave, but shows a phase difference in its pitch angle; in our study, there is no detectable phase difference between body wave and tail wave, and the tail behaves like an extension of the body wave. (3) Size of amplitude envelope relative to the width of the head (Fig. 4, inset): the mullet's anterior body is wider or about as wide as the body wave amplitude along most of the body. As a consequence, the body contour on the convex side is almost straight and hardly exceeds the head contour, while the body contour on the concave side of the bend is curved and recedes substantially beyond the head contour. This asymmetry exists independent of the slip and causes considerable differences between the flow fields in concave and convex bends.

Slip and wake shape

In all sequences analysed, the shed vortices resemble a Rankine vortex profile, whose hypothetical structure consists of a core in solid-body rotation and an outer potential flow region entrained by the core (Fig. 3).

A fish swimming with a slip below 1.0 sheds two rows of alternating vortices with a backward jet in-between (Fig. 2A, B). Per tail beat cycle, one clockwise vortex is shed to the left and one counter-clockwise vortex to the right. At a slip of 0.7, the angle α between the jet and the mean path of motion is 45 ± 7.5° (n = 61), and the cores of the vortices have an approximately circular shape (Fig. 2A). At a slip of 0.9, the jet angle α is 61 ± 9.5° (n = 19), and the cores of the vortices are slightly more elongated perpendicular to the mean path of motion (Fig. 2B). At a slip of 1.1, indicating that the fish is decelerating, the wake initially looks rather similar to the wake of an actively swimming fish (Fig. 2C). However, over a time period of 0.3 sec, the vortices, shed as single round vortices, stretch out (vortex 2 to 4 in Fig. 2C *vs.* 2D) and two vortex cores emerge (vortex 3 and 4a,b, Fig. 2D). The mature wake resembles a single row of oval vortices with jets almost perpendicular to the path of motion (α: 75 ± 14.0°, n = 43) (Fig. 2D).

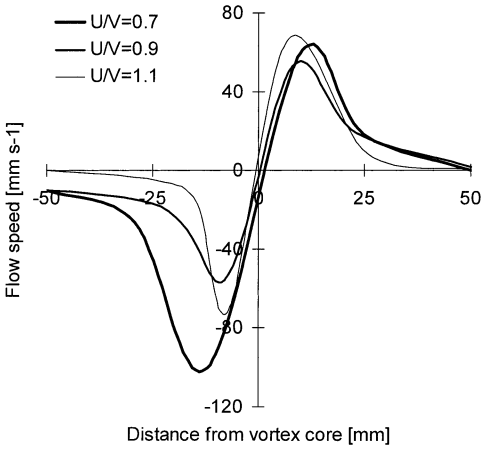

FIG. 3. Velocity profiles of the following vortices (0.12 sec after being shed). *U*/*V* = 0.7: profile of vortex 2 in Fig. 2A. *U*/*V* = 0.9: profile of vortex 2 in Fig. 2B. *U*/*V* = 1.1: profile of vortex 3 in Fig. 2C and D.

Slip and positioning of the vortices: the influence of the tail

Independent of the slip, vortices are shed at the tail when the tail reaches its maximum lateral excursion. The spacing of the vortex centres reflects the undulating path of the tail (Fig. 2 insets). The distance between consecutive vortex centres along the mean path of motion corresponds to half the stride length (Table 2). The distance between the vortex centres perpendicular to the mean path of motion is close to twice the tail beat amplitude (Table 2). The vortices stay at the position where they were shed by the tail, however, the initial shedding pattern is obscured in the mature wake at slips close to 1 due to the considerable changes in the vortex shape (Fig. 2B–D).

Slip and vortex interaction: the influence of the body

The body wave creates strong semicircular flows: suction flows toward the body adjacent to the concave bends, and positive pressure flows away from the body in the convex bends. The flow speeds created in the concave bends are higher than the speeds in the convex bends, for all slips (Fig. 4) (Müller *et al.*, 1997). This difference is caused by the asymmetry of the lateral body movements (Fig. 4, inset). The centres of rotation of these semicircular flows travel down the body (Fig. 4). Their path depends on the slip: at a slip of 0.7, the rotational centres travel close to the maxi-

TABLE 2. *Wake morphology.**

	Sequence 1	Sequence 2	Sequence 3
vortex spacing across PoM** λ_Y (m)	0.016 ± 0.007 (58)	0.019 ± 0.008 (19)	0.017 ± 0.010 (12)
vortex spacing along PoM** λ_X (m)	0.032 ± 0.010 (62)	0.029 ± 0.009 (19)	0.032 ± 0.005 (12)
ring momementum angle φ (deg)	40 ± 10 (55)	35 ± 14 (18)	29 ± 13 (9)
vortex core radius R_0 (m)	0.012 ± 0.007 (16)	0.007 ± 0.001 (7)	0.015 ± 0.005 (12)
vortex ring radius R (m)	0.016 ± 0.003 (16)	0.019 ± 0.005 (4)	0.018 ± 0.003 (7)
jet angle α (deg)	44 ± 7 (61)	61 ± 10 (19)	75 ± 14 (43)
circulation Γ ($mm^2\ s^{-1}$)	521 ± 38 (5)	432 ± 122 (3)	430 ± 65 (8)
thrust power P_T (mW)	0.11 ± 0.04 (5)	0.10 ± 0.03 (3)	0.09 ± 0.01 (8)

* All means are derived from vortices that were shed 0 to 0.4 s ago. Circulation and power are based on a more narrow time window of 0.04 to 0.12 s since shedding.

** PoM: path of motion.

mum of the body wave amplitude envelope, and the flow past the body forms a 'body wake' close to the place and time when the tail sheds its wake; as slip decreases, so does the lateral offset of the rotational centres, and the separation between body and tail vortices released into the wake becomes larger.

Energy in the wake. Neither the angular velocities of the vortex cores nor the velocities in the jet differ dramatically for the three sequences considered (Table 2). The circulation of the vortices just after being shed is highest at the lowest slip of 0.7, when body- and tail wake combine, compared to the strength of the split vortices at a slip of 1.1. However, the size and the total momentum of the wake are quite similar. With both the generated flow velocities and the affected water mass being similar in all three sequences, this suggests that the total momentum shed by the fish does not change substantially with increasing slip, but rather that the proportion of backward momentum decreases drastically. At a slip of 1.1 this low backward momentum is reflected in the high angles α between jet flow and mean path of motion, and the low momentum angle of the vortex rings φ (Fig. 2D, Table 2). At a slip of 0.7, the jet angle and the momentum angle are both close to 45°; significant backward momentum is present in the wake and consequently the fish gains considerable forward momentum (Fig. 2A, Table 2).

DISCUSSION

Wake generation: contributions of body and tail

Fish accelerate the water adjacent to the body for propulsion. The increase of local flow speeds can provide a rough estimate of the contribution from body and tail to the total momentum imparted to the wake: the flow velocities increase slowly along the first two thirds of the body; in the tail region, flow velocities almost double (Fig. 4) (Müller *et al.*, 1997). The body accelerates the local flow to roughly half the maxi-

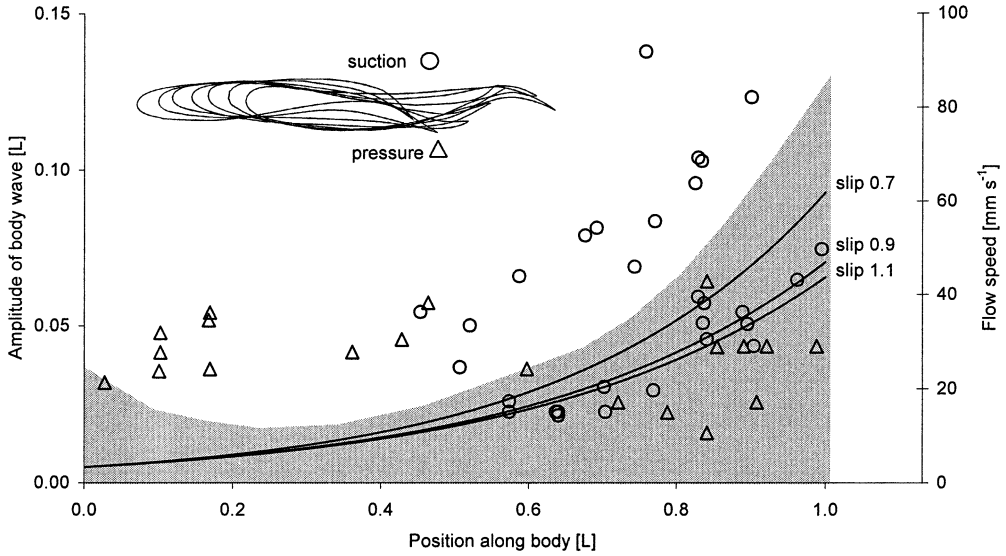

FIG. 4. Flow speeds (circles and triangles) and position of the pressure nodes (lines) along the mullet and relative to the amplitude envelope (grey area) over a complete tail beat cycle. The lines are an exponential fit through all pressure nodes at each slip. The exponent of the fit increases as slip decreases, indicating that the nodes travel closer to the edge of the amplitude envelope at lower slip values. The flow speeds at a particular position along the body can range from values close to zero, when the body segment in question is close to a pressure node, to maximum when the segment is in the suction or pressure zone. Figure 4 inset: superimposed body contours of a swimming mullet (U = 0.17 m; U/V = 0.7). On the convex or pressure side (triangle) of the body wave, the body extends little beyond the head contour, while on the concave or suction side (circle) of the body wave, the body recedes considerably.

mum, and the tail completes the acceleration to final flow speeds measured at the tail tip and in the jet.

Undulatory swimming can be conceptualised as the action of two waving plates, one plate being positioned in the wake of the other plate. The tail corresponds to the downstream waving plate. The tail acts like an oscillating hydrofoil, contributing to the shape of the wake and the momentum shed: the position of the vortices shed in the wake behind a swimming mullet reflects the path of the tail tip (Fig. 2). The body is the upstream waving plate: its wake interacts with the tail and modifies the tail's hydrodynamic performance; the body undulations generate semi-circular flow patterns adjacent to the body that, upon reaching the tail, cause the shedding of body-generated vorticity. The interaction between this body-generated vorticity and the tail wake depends on the phase relationship between the two wakes (Gopalkrishnan *et al.,* 1994). This phase relationship depends on the slip. At the highest slip of 1.1, the body- and tail wakes are shed far enough apart to generate a wake with split-core vortices (Fig. 2C, D). When the phase between body wake and tail wake is altered so that the body-generated vorticity is shed at the same moment as the tail generated vorticity, then the two wakes combine: tail- and body-generated vortices merge into one vortex (Fig. 2A). We also observed an intermediate case at a slip of 0.9 in which the two vortices seem to merge incompletely, generating a rather oval-shaped combined vortex core (Fig. 2B).

To support the claim that phase between the body wave and tail beat cycle, and hence the wake interaction, depends on the slip, we used Lighthill's slender body theory (1960) as a simple analytical model to predict the position of the body wake (Müller *et al.*, 2001). More sophisticated flow models have been published that demonstrate that swimming performance and wake shape strongly depend on the body wave characteristics (Cheng *et al.*, 1991; Cheng and Blickhan, 1994; Pedley and Hill, 1999; Triantafyllou *et al.*, 2000). We assume in our simple analytical model of the body wake that the body-generated flows, which are ultimately shed as the body-vortex, first travel down the body with a ''vortex'' core at the point where the pressure gradient, and hence the lift, is zero. Using Lighthill's slender body theory to estimate the position of this pressure node, we find that the nodes reach the tail at lateral positions that depend on the slip (Fig. 4). The body vortex's shedding pattern responds most strongly to small changes in slip around slip values of 1 (Fig. 5). At a slip of 1, the analytical model predicts that the body vortices are shed on the path of motion, maximising the distance between body- and tail vortices. As slip decreases, so does the distance between the two types of vortex, until they coincide at a slip of around 0.7. The predictions from this simple model suggest that undulatory swimmers can control the interaction between body- and tail wake, and that this would afford them control over their swimming performance. The phase between body- and tail wake depends not only on the slip, but also on the amplitude envelope. A steeper curvilinear increase of the body wave amplitude envelope reduces the slip value at which body- and tail wake are in phase: the eel-like amplitude envelope (Fig. 5 top) causes the distance between shed body- and tail vortices to exhibit minima at higher slips than the mullet-like amplitude envelope (Fig. 5 bottom).

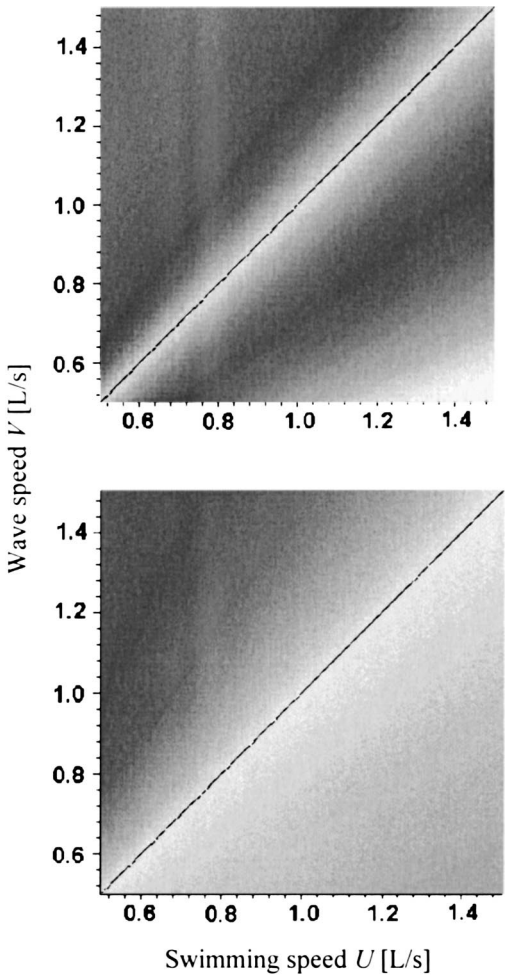

FIG. 5. Predicted distance between tail- and body vortex at the moment of shedding as a function of swimming speed U and body wave speed V for (top) anguilliform and (bottom) carangiform amplitude envelopes. The dark line along the white crest indicates slip = 0. The darkest greys indicate a distance of zero. The white crests indicate distances equivalent to the tail beat amplitude.

Even though the body wake of mullet seems to be considerably weaker than the body wake of an eel, our flow fields and analytical models suggest that nevertheless it affects propulsive performance considerably by its interaction with the tail wake. While the tail kinematics seem to determine the positioning of the vortices in the (young(wake, the emergence of split vortices in the mature wake suggests that the shedding of a weaker wake from the body reshapes the total wake, as tail wake and body wake interact.

ACKNOWLEDGMENTS

The swimming sequences were recorded by B. L. E. van den Heuvel under the supervision of U. K. Müller. We would like to thank the Sea Life Centre in Schevingen, The Netherlands, for providing the two mullets, and BASF for providing the polystyrene particles. Eric Tytell's and Otto Berg's help with the analytical body wake model was invaluable. Jim Usherwood helped to improve the English.

REFERENCES

Ahlborn, B., D. G. Harper, R. W. Blake, D. Ahlborn, and M. Cam. 1991. Fish without footprints. J. Theor. Biol. 148:521–533.

Aleyev, Y. G. 1977. *Nekton.* Dr. W. Junk, The Hague.

Anderson, J., K. Streitlien, D. Barret, and M. Triantafyllou. 1998. Oscillating foils of high propulsive efficiency. J. Fluid Mech. 360:41–72.

Blickhan, R., C. Krick, D. Zehren, and W. Nachtigall. 1992. Generation of a vortex chain in the wake of a subundulatory swimmer. Naturwissenschaften 79:220–221.

Cheng, J.-Y., L.-X. Zhuang, and B.-G. Tong. 1991. Analysis of swimming three-dimensional waving plates. J. Fluid Mech. 232: 341–355.

Cheng, J.-Y. and R. Blickhan. 1994. Bending moment distribution along swimming fish. J. Theor. Biol. 168:337–348.

Chen, C. J., Y. G. Kim, and J. A. Walter. 1993. Progress in Quantitative flow visualisation and imaging process. *In* The Visualization Society of Japan (ed.), *Atlas of visualisation,* pp. 279–296. Pergamon Press, Oxford.

Drucker, E. G. and G. V. Lauder. 1999. Locomotor forces on swimming fish: Three-dimensional vortex wake dynamics quantified using digital particle velocimetry. J. Exp. Biol. 202:2393–2412.

Drucker, E. G. and G. V. Lauder. 2001. Locomotor function of the dorsal fin in teleost fishes: Experimental analysis of wake forces in sunfish. J. Exp. Biol. 204:2943–2958.

Gray, J. 1968. *Animal locomotion.* Weidenfeld and Nicholsen, London.

Hanke, W., C. Brucker, and H. Bleckmann. 2000. The ageing of the low-frequency water disturbances caused by swimming goldfish and its possible relevance to prey detection. J. Exp. Biol. 203: 1193–1200.

Hertel, H. 1966. *Structure, form, movement.* Reinhold Publishing Corp., New York.

Lighthill, M. J. 1960. Note on swimming of slender fish. J. Fluid Mech. 9:305–317.

Müller, U. K., B. L. E. van den Heuvel, E. J. Stamhuis, and J. J. Videler. 1997. Fish foot prints: Morphology and energetics of the wake behind a continuously swimming mullet (*Chelon labrosus*). J. Exp. Biol. 200:2893–2906.

Müller, U. K., J. Smit, E. J. Stamhuis, and J. J. Videler. 2001. How the body contributes to the wake in undulatory fish swimming: Flow fields of a swimming eel (*Anguilla anguilla*). J. Exp. Biol. 204:2751–2762.

Nauen, J. C. and G. V. Lauder. 2001. Locomotion in scombrid fishes: Visualization of flow around the caudal peduncle and finlets of the chub mackerel *Scomber japonicus*. J. Exp. Biol. 204(13): 2251–2263.

Pedley, T. J. and S. J. Hill. 1999. Large amplitude undulatory fish swimming: Fluid mechanics coupled to internal mechanics. J. Exp. Biol. 202:3431–3438.

Rayner, J. M. V. 1979. A vortex theory of animal flight mechanics. J. Fluid Mech. 91:731–763.

Rosen, M. W. 1959. *Water flow about a swimming fish.* U.S. Naval Ordnance Test Station TP 2298, China Lake, California.

Spedding, G. R., J. M. V. Rayner, and C. J. Pennycuick. 1984. Momentum and energy in the wake of a pigeon (*Columbia livia*) in slow flight. J. Exp. Biol. 111:81–102.

Stamhuis, E. J. and J. J. Videler. 1995. Quantitative flow analysis around aquatic animals using laser sheet particle image velocimetry. J. Exp. Biol. 198:283–294.

Triantafyllou, M. S., G. S. Triantafyllou, and M. A. Grosenbaugh. 1993. Optimal thrust development in oscillating foils with application to fish propulsion. J. Fluid and Structures 7:205–224.

Triantafyllou, M. S., G. S. Triantafyllou, and D. K. P. Yue. 2000. Hydrodynamics of fishlike swimming. Ann. Rev. Fluid Mech. 32:33–53.

Videler, J. J. 1993. *Fish swimming.* Chapman and Hall, London.

Vollmers, H. 1993. Strömungsfelder analysieren, darstellen und interpretieren. DLR Nachrichten 70:2–8.

Wardle, C. S., J. J. Videler, and J. D. Altringham. 1995. Tuning in to fish swimming waves: body form, swimming mode and muscle function. J. Exp. Biol. 198:1629–1636.

Wilga, C. D. and G. V. Lauder. 2000. Three-dimensional kinematics and wake structure of the pectoral fins during locomotion in leopard sharks *Triakis semifasciata*. J. Exp. Biol. 203:2261–2278.

Wolfgang, M. J., J. M. Anderson, M. A. Grosenbaugh, D. K. P. Yue, and M. S. Triantafyllou. 1999. Near-body flow dynamics in swimming fish. J. Exp. Biol. 202:2303–2327.